Experiments and Calculations on Rate Coefficients for Pyrolysis of SO_2 and the Reaction O + SO at High Temperatures

Chih-Wei Lu,[†] Yu-Jong Wu,[†] and Yuan-Pern Lee*[,†,‡]

Department of Chemistry, National Tsing Hua University, 101, Sec. 2, Kuang Fu Road, Hsinchu 30013, Taiwan, and Institute of Atomic and Molecular Sciences, Academia Sinica, Taipei, Taiwan

R. S. Zhu and M. C. Lin*

Department of Chemistry, Emory University, Atlanta, Georgia 30322

Received: July 14, 2003; In Final Form: September 22, 2003

Rate coefficients for the pyrolysis of SO_2 in Ar in the temperature range 2188−4249 K were determined using a diaphragmless shock tube. The concentration of O atoms was monitored with resonance absorption. Rate coefficients determined in this work show Arrhenius behavior, with $k_{1a}(T) = (4.86 \pm 1.31) \times 10^{-9}$ exp $[-(50450 \pm 730)/T]$ cm^3 molecule^{-1} s^{-1}; listed errors represent one standard deviation in fitting. These values are consistent with some previous measurements that show a preexponential factor and activation energy greater than other measurements. Theoretical calculations at the G2M(RCC2) level, using geometries optimized with the B3LYP/6-311+G(3df) method, yield energies of transition states and products relative to those of the reactants. Rate coefficients predicted with a microcannonical variational RRKM theory agree well with experimental observations; contributions from electronically excited states of SO_2 are significant. Rate coefficients for the recombination O + SO → SO_2 are predicted to decrease with temperature with $k_{10a}(T) = (4.82 \pm 0.05) \times 10^{-31}(T/298)^{-2.17\pm0.03}$ cm^6 molecule^{-2} s^{-1} for the temperature range 298−3000 K. In some experiments, S atoms were monitored with resonance absorption. With detailed chemical modeling, we found that S atoms were mainly produced from the secondary reaction O + SO → S + O_2 rather than from direct pyrolysis of SO_2 or from further pyrolysis of the SO product. Rate coefficients for this secondary reaction, determined to be $k_{10b}(T) = (3.0 \pm 0.3) \times 10^{-11}$ exp $[-(6980 \pm 280)/T]$ cm^3 molecule^{-1} s^{-1}, agree closely with the theoretically predicted value comprising three product-channels via one triplet and two singlet SOO intermediates.

1. Introduction

SO_2 is a key species in oxidation reactions of sulfur compounds that are important in atmospheric and combustion chemistry. In experiments at high-temperatures, SO_2 is commonly employed as a source of O atoms. The kinetics for the thermal decomposition of SO_2 has, however, a controversial history. Previous rate measurements in the temperature range of 2500−7500 K all employed shock-wave techniques, from which reported rate coefficients fall into roughly three groups, as listed in Table 1. Earlier experiments[1,2] using SO_2 at larger concentrations yield rate coefficients k_{1a} showing activation energies, $E_a = R(28200-37700\ \text{K}) = 56.0-74.9$ kcal mol^{-1}, much smaller than the bond energy for O−SO

$$SO_2 \rightarrow O(^3P) + SO(^3\Sigma^-) \quad \Delta H^\circ = 131.8 \text{ kcal mol}^{-1} \quad (1a)$$

Other reported rate coefficients all exhibit similar activation energies in the range $100.3 < E_a/\text{kcal mol}^{-1} < 116.4$ (50500 K $< E_a/R <$ 58600 K), but with values differing by a factor as much as 50 at a specific temperature in the range 3000−5000 K. Experiments involving detection of SO_2 through ultraviolet (UV) absorption or emission invariably yielded smaller rate coefficients.[3−5] Plach and Troe[6] showed that these measurements were in error because UV absorption spectra of SO and SO_2 overlap extensively; observed results of smaller rate coefficients are therefore attributed to interference from the absorption of SO.

Experiments using a laser schlieren technique,[7,8] atomic resonance absorption of O atoms,[9] infrared (IR) emission of SO_2,[10] and UV absorption of SO_2 at $\lambda \leq 220$ nm (ref 6) gave reasonably consistent results with greater values of rate coefficients. On close inspection, reported E_a/R values still vary by ∼16%, and preexponential factors vary by nearly a factor of 10, from 5.55×10^{-9} to 4.82×10^{-8} cm^3 molecule^{-1} s^{-1}. Other reaction channels such as

$$SO_2 \rightarrow S\ (^3P) + O_2\ (^3\Sigma_g^-) \quad \Delta H^\circ = 137.3 \text{ kcal mol}^{-1} \quad (1b)$$

$$SO_2 \rightarrow SOO \quad \Delta H^\circ \cong 110 \text{ kcal mol}^{-1} \quad (2)$$

have never been investigated. Hence, we sought to examine carefully the pyrolysis reaction of SO_2 and associated secondary reactions in our newly constructed diaphragmless shock tube by probing both O and S atoms with atomic resonance absorption as part of extensive investigations concerning reactions of SO_x.

Pyrolysis of SO_2 has never been studied theoretically. The system is complicated because it involves atoms (S and O) in

* To whom correspondence should be addressed. (Y.P.L.) E-mail: yplee@mx.nthu.edu.tw. Fax: 886-3-572-2892. (M.C.L.) E-mail: chemmcl@emory.edu. Fax: 1-404-727-6586.

[†] National Tsing Hua University.

[‡] Academia Sinica.

10.1021/jp036025c CCC: $25.00 © 2003 American Chemical Society
Published on Web 11/20/2003

TABLE 1: Comparison of Reported Temperature Dependence of Rate Coefficients and Experimental Conditions for Pyrolysis of SO_2

temp, K	pressure, 10^{17}[a]	[SO2]/[M]	M	A_0, 10^{-10} [b]	E_a/R, K	detection method	ref
2188−4249	10.5−37.9	100−900 ppm	Ar	48.6 ± 13.1	50450 ± 730	O absorption at 130.2 ± 1.4 nm	this work
2000−4500			Ar	471	55190	theory (Arrhenius fit for the listed T range)	this work
3000−5000		800−6000 ppm	Ar	66.1	50510 ± 3970	SO_2 absorption, $\lambda \leq 220$ nm	PT[6]
4000−6000		0.06−0.20	Ar	55.5	54150	Laser Schlieren at 632.8 nm	RBR[8]
		1.00	SO_2	8.34	33520		
4300−6200	4.52−13.8	20 & 100 ppm	Ar	5.89	52800	SO_2 emission at 392.5 nm	SYM[5]
2800−3880	48−205	0.0013−0.00527	Ar	133 ± 33	54350	SO_2 emission 7.26−7.47 μm	GRS[10]
2500−3400		20−200 ppm	Ar	$482 \pm {}^{572}_{262}$	58590 ± 2270	O absorption at 130.5 nm SO absorption at 146.9 nm	JR[9]
3300−6500	30−403	100−2000 ppm	Ar	$6.61 \pm {}^{6.59}_{3.30}$	53880 ± 2170	SO_2 absorption at 227 ± 0.2, 234 ± 0.2, and 238.5 ± 0.2 nm SO absorption at 219.5 ± 0.13 nm SO_2 emission at 7.25 ± 0.30 μm SO emission at 275 ± 1 & 316.5 ± 0.5 nm	AGT[4]
2900−5200	4.52−60.2	0.03, 0.10, 0.30	Kr	282	56360 ± 2010	laser schlieren at 632.8 nm	Kiefer[7]
2800−3400	2.56−12.0	0.01−0.40	Ar	1.33 ± 0.27[c]	37740 ± 2010	SO emission at 436 ± 8 nm	LS[2]
3000−4000	60.2−482	0.0036−0.01	SO_2	16.6	35230 ± 3520	SO_2 absorption 210−330 nm	OTW[3]
4500−7500		0.0005−0.01	Ar	4.17	55360	SO_2 absorption 210−330 nm	OTW[3]
3004−3978	5.06−23.5	0.04−0.32	Ar	0.106 ± 0.012	28180 ± 3020	SO absorption 254.8, 258.1, 262.2 nm	GKP[1]

[a] In unit of molecule cm^{-3}. [b] In unit of cm^3 $molecule^{-1}$ s^{-1}. [c] An intercept at [M] = 0 was taken out.

their triplet states and molecules (SO, SO_2, and O_2) in various singlet and triplet states. The role of electronically excited SO_2 in enhancing the rate of decomposition was previously proposed.[6,9]

We have performed a careful experimental work on the decomposition of SO_2 and extended rate measurements down to 2188 K. The mechanism for production of S atoms has been clarified to be due to the secondary reaction O + SO. We also performed detailed theoretical calculations to predict rate coefficients for both forward and reverse reactions and confirmed the important role of triplet SO_2 in this reaction. The theoretically predicted rate coefficient for O + SO → S + O_2 also agrees well with experiments.

2. Experiments

Details of the diaphragmless shock tube apparatus have been reported.[11,12] The shock tube (length 5.9 m and internal diameter 7.6 cm) is coupled to a detection system using atomic resonance absorption. Three time-frequency counters were employed to determine the speed of the shock wave based on signals detected with sensors installed at 3, 20, 30, and 40 cm from the end of the tube. A microwave discharge of a flowing gas mixture of O_2 ~1.0% in He served as a lamp for atomic absorption of O atoms. Overlapped emission of the lamp at 130.22, 130.49, and 130.60 nm, corresponding to atomic transitions of $O(^3S)-O(^3P_{2,1,0})$, passes through the shock tube to a vacuum UV monochromator (focal length 20 cm, reciprocal linear dispersion 4.0 nm mm^{-1}, slit width 350 μm) before being detected with a solar-blind photomultiplier tube. Variation of the signal from the photomultiplier was monitored with a digital storage oscilloscope and transferred to a computer for further processing. In a few experiments, S atoms were monitored with absorption at 180.73, 182.03, and 182.62 nm, corresponding to atomic transitions of $S(^3S)-S(^3P_{2,1,0})$, from microwave discharge of a mixture of SO_2 ~0.10% in He.

Before each experiment, the shock tube was pumped below 5.0×10^{-7} Torr. The temperature (T_5), density (ρ_5), and pressure (P_5) in the reflected shock regime were calculated from the measured velocity of the incident shock, the composition of the test gas, the initial pressure, and the temperature according to the ideal shock-wave theory;[13] Mirels' boundary-layer corrections were negligible under high temperature and with large Mach number.[14,15]

We calibrated the concentration of O atoms in the shock tube with N_2O, assuming a 100% yield of O atoms from pyrolysis of N_2O. Similarly, the concentration of S atoms was calibrated with OCS pyrolysis; the absorption cross section of S atoms depends on pressure.

Ar (99.9995%, AGA Specialty Gases), N_2O (99%, Scott Specialty Gases), OCS (99.98%, Matheson), and SO_2 (99.98%, Matheson) were used without further purification. Mixtures of SO_2 in Ar (100−900 ppm), OCS in Ar (5.0−25.1 ppm), and N_2O in Ar (10.0−30.4 ppm) were used.

3. Computational Methods

The geometries of the reactant, intermediates, transition states, and products of the SO_2 decomposition system were optimized at the B3LYP/6-311+G(3df) level of theory with Becke's three-parameter nonlocal exchange functional[16] and the nonlocal correlation functional of Lee et al.[17] Energies of all species were calculated at the G2M(RCC2) level of theory[18] using geometries optimized with the B3LYP/6-311+G(3df) method. Intrinsic reaction coordinate (IRC) calculations[19] were performed to connect each transition state with designated reactants and products. All calculations were carried out with Gaussian 98[20] and MOLPRO 2002 programs.[21]

The structures of the low lying electronically excited states involved in the reaction were optimized at the RB3LYP/6-311+G(3df) or UB3LYP/6-311+G(3df) level. As some investigators[22−24] have shown, for systems with multireference characters, density functional theory can predict molecular properties reasonably. For the low-lying states of SO_2, Katagiri et al.[25] showed that A $^1A_2$, a $^3B_1$, and b $^3A_2$ states can be dominantly constructed by the configuration of the electronic ground state X $^1A_1$ with the electronic configuration $...(2b_1)^2-(1a_2)^2(5b_2)^2(8a_1)^2$. Excited-state electronic configurations were derived from the excitation of the electrons in the $8a_1$, $1a_2$, and $5b_2$ occupied orbitals to the $3b_1$ unoccupied orbital. The ground-state structure obtained at the B3LYP/6-311+G(3df) level was used as the initial input to construct the specific configurations. For SO_2 ($^1A_2$), SOO ($^1A''$), and their triplet states, as well as their related transition states, the unrestricted wave functions were used. The constructed configurations and symmetry were kept unchanged in the process of geometry optimization and single energy calculations with the G2M method.

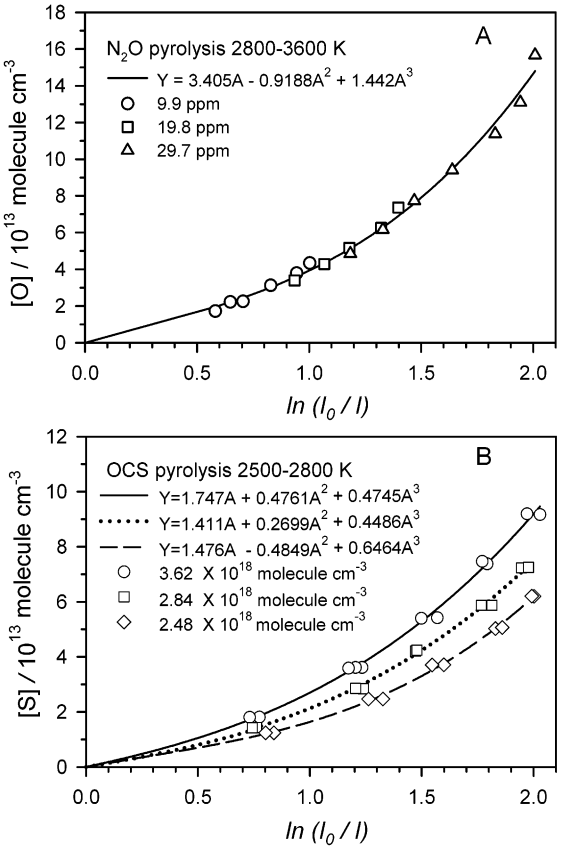

Figure 1. (A) Calibration curve of [O] versus absorbance of O atoms; (B) Calibration curve of [S] versus absorbance of S atoms at total pressures of 3.62 (○), 2.84 (□), and 2.48 (◇) $\times 10^{18}$ molecule cm^{-3}. Fitted equations are listed in the legends.

Rate coefficients for various reaction channels were calculated with a microcannonical variational RRKM method using the Variflex program.[26] The component rates were evaluated at E,J-resolved levels. The master equation was solved with inversion and eigenvalue-based approaches for association and dissociation processes, respectively.[27,28] For the barrierless transition state, we used a Morse potential

$$E(R) = D_e[1 - e^{-\beta(R-R_e)}]^2 \quad (3)$$

in which D_e is the dissociation energy (D_0) plus zero-point energy, R_e is the equilibrium bond distance, and β is fitted from calculated potential energies at discrete atomic separations R, to represent the potential curve along the minimum energy path of each individual reaction coordinate. For tight transition states, the numbers of states were evaluated with a rigid-rotor harmonic-oscillator approximation.

4. Results and Discussion

4.1. Calibrations of [O] and [S]. Calibration of [O] using thermal decomposition of N_2O is a standard procedure in the shock-tube technique;[29] it takes into account deviations from the Beer−Lambert law. The calibration curve of [O] using various concentrations of N_2O is shown in Figure 1A. Absorbance A is calculated with the equation

$$A = \ln(I_0/I) \quad (4)$$

in which the light intensity before and after production of O atoms is denoted as I_0 and I, respectively. The concentration of O atoms is fitted with an equation

$$[O]/10^{13}\ \text{molecule cm}^{-3} = 3.405A - 0.9188A^2 + 1.442A^3 \quad (5)$$

for a total pressure (1.63−5.28) $\times$ 10^{18} molecule cm^{-3}.

Calibration of [S] was carried out similarly by the thermal decomposition of OCS at high temperatures.[30,31] The concentration of S atoms, (1.24−9.20) $\times$ 10^{13} molecule cm^{-3}, was fitted with various quadratic equations depending on the total pressure for concentrations in the range (2.48−3.62) $\times$ 10^{18} molecule cm^{-3}, as shown in Figure 1B. At a total concentration of 3.62 $\times$ 10^{18} molecule cm^{-3}, the concentration of S atoms is fitted with an equation

$$[S]/10^{13}\ \text{molecule cm}^{-3} = 1.747A + 0.4761A^2 + 0.4745A^3 \quad (6)$$

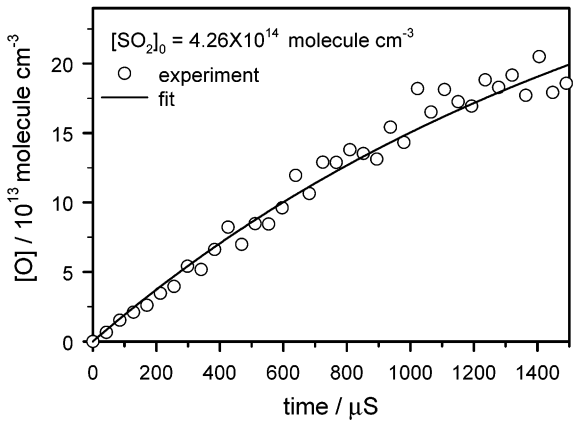

Figure 2. Temporal profiles of [O] observed for pyrolysis of an Ar sample containing SO_2 (200.1 ppm). $T = 2831$ K and $P = 2.12 \times 10^{18}$ molecule cm^{-3}. The solid line represents fitted results using the model described in text.

4.2. Rate Coefficient k_{1a} of the Reaction $SO_2 \rightarrow O + SO$. Figure 2 shows a typical temporal profile of [O] observed when a gas mixture containing SO_2 and Ar was heated with a shock wave. The concentration of O atoms at reaction time t, $[O]_t$, is derived according to eqs 4 and 5, with the light intensity before pyrolysis taken as I_0 . If reaction 1a were the sole pyrolysis channel and there were no interference reaction, a temporal profile of $[O]_t$ can be fitted to a first-order equation to yield a pseudo-first-order rate coefficient k^I

$$[O]_t = [SO_2]_0\,[1 - \exp(-k^I t)] \quad (7)$$

The apparent second-order rate coefficient, k'_{1a}, is thus derived from

$$k'_{1a} = k^I/[Ar] \quad (8)$$

At high temperatures, these secondary reactions involving O, SO, and O must be considered

$$O + SO_2 \xrightarrow{M} SO_3 \quad (9a)$$

$$\rightarrow SO + O_2 \quad (9b)$$

$$O + SO \xrightarrow{M} SO_2 \quad (10a)$$

$$\rightarrow S + O_2 \quad (10b)$$

$$O + O \xrightarrow{M} O_2 \quad (11)$$

$$SO + SO \rightarrow S + SO_2 \quad (12)$$

$$SO \xrightarrow{M} S + O \quad (13)$$

$$O + SO_3 \rightarrow O_2 + SO_2 \quad (14)$$

for which rate coefficients have the reported dependence on temperature

$$k_{9a}(T) = 1.21 \times 10^{-33} \exp(3163/T)\ \text{cm}^6\ \text{molecule}^{-2}\ \text{s}^{-1} \quad \text{(ref 32)} \quad (15)$$

$$k_{9b}(T) = 8.3 \times 10^{-12} \exp(-9800/T)\ \text{cm}^3\ \text{molecule}^{-1}\ \text{s}^{-1} \quad \text{(ref 33)} \quad (16)$$

$$k_{10a}(T) = 3.3 \times 10^{-26}\, T^{-1.84}\ \text{cm}^6\ \text{molecule}^{-2}\ \text{s}^{-1} \quad \text{(ref 10)} \quad (17)$$

$$k_{10b}(T) = 3.63 \times 10^{-11} \exp(-7700/T)\ \text{cm}^3\ \text{molecule}^{-1}\ \text{s}^{-1} \quad (18)$$

$$k_{11}(T) = 5.21 \times 10^{-35} \exp(900/T)\ \text{cm}^6\ \text{molecule}^{-2}\ \text{s}^{-1} \quad \text{(ref 34)} \quad (19)$$

$$k_{12}(T) = 4.73 \times 10^{-13} \exp(-880/T)\ \text{cm}^3\ \text{molecule}^{-1}\ \text{s}^{-1} \quad \text{(ref 35)} \quad (20)$$

$$k_{13}(T) = 6.61 \times 10^{-10} \exp(-53890/T)\ \text{cm}^3\ \text{molecule}^{-1}\ \text{s}^{-1} \quad \text{(ref 6)} \quad (21)$$

$$k_{14}(T) = 2.19 \times 10^{-12} \exp(-3070/T)\ \text{cm}^3\ \text{molecule}^{-1}\ \text{s}^{-1} \quad \text{(ref 32)} \quad (22)$$

in which k_{10b} was estimated from reported rate coefficients of the reverse reaction (2732−3463 K)[36] and the equilibrium constant derived from literature values of $\Delta G(T)$ for corresponding species.[37] Values of k_{12} might have large errors because there is only one study at high temperature (1000 K), and we estimate the activation energy based on reported values at 1000 and 298 K.[35] We modeled observed temporal profiles of [O] with reactions 1a and 9−14 using a commercial kinetic modeling program FACSIMILE;[38] rate coefficients listed in eqs 15−22 were held constant, and the second-order rate coefficient of the title reaction, k_{1a}, was varied to yield the best fit. Experimental conditions and values of k_{1a} for 48 measurements involving SO_2 at five initial concentrations (in a range 100−900 ppm in Ar) within the temperature range 2188−4249 K are summarized in Table 2; we also list k_{1a}/k'_{1a} for comparison. Values of k'_{1a} obtained with eq 8 based on pseudo-first-order kinetics deviate from k_{1a} by less than 20% (<4% for mixtures with $[SO_2] \leq 200$ ppm), indicating that secondary reactions play only a minor role under our experimental conditions. Detailed modeling shows that secondary reactions are negligible at high temperatures because reaction 1a increases much more rapidly than possible interfering reactions, whereas at low temperatures and greater $[SO_2]$, reaction 9b is the only interfering reaction accounting for more than 3% of correction, with a maximal contribution ~14 % to k_{1a} under our experimental conditions. We also used the theoretically predicted value of k_{10a} (to be discussed in section 4.5) and the experimental value of k_{10b} (to be discussed in section 4.3) to replace values listed in eqs 17 and 18 in the model and derived nearly identical values of k_{1a}.

TABLE 2: Experimental Conditions and Rate Coefficient k_{1a} for Pyrolysis of SO_2 to Form SO + O[a]

P_1/ Torr	P_4/ Torr	M_s	T_5/ K	$[SO_2]$/ 10^{14}	[Ar]/ 10^{18}	k_{1a}/ $cm^3\ molecule^{-1}s^{-1}$	k_{1a}/k_{1a}'
				SO_2 (100.0 ppm)			
9.08	2250	3.65	3116	2.20	2.20	$(4.16 \pm 0.08) \times 10^{-16}$	1.010
8.05	2250	3.72	3239	1.97	1.97	$(7.55 \pm 0.14) \times 10^{-16}$	1.030
7.52	2250	3.79	3361	1.86	1.86	$(1.27 \pm 0.02) \times 10^{-15}$	0.996
7.07	2250	3.85	3449	1.76	1.76	$(3.35 \pm 0.05) \times 10^{-15}$	0.997
5.86	2250	3.90	3541	1.47	1.47	$(5.56 \pm 0.09) \times 10^{-15}$	0.998
5.61	2250	3.97	3664	1.42	1.42	$(4.57 \pm 0.11) \times 10^{-15}$	0.990
5.55	2250	4.00	3718	1.41	1.41	$(9.93 \pm 0.20) \times 10^{-15}$	0.990
5.53	2500	4.09	3890	1.42	1.42	$(1.29 \pm 0.03) \times 10^{-14}$	0.993
5.02	2500	4.13	3960	1.29	1.29	$(2.43 \pm 0.04) \times 10^{-14}$	0.987
4.42	2500	4.20	4084	1.15	1.15	$(1.74 \pm 0.03) \times 10^{-14}$	0.993
4.34	2500	4.23	4138	1.13	1.13	$(2.17 \pm 0.05) \times 10^{-14}$	0.981
4.02	2500	4.29	4249	1.05	1.05	$(3.83 \pm 0.09) \times 10^{-14}$	0.972
				SO_2 (200.1 ppm)			
13.05	2000	3.24	2494	5.90	2.95	$(1.10 \pm 0.03) \times 10^{-17}$	1.039
12.51	2000	3.29	2559	5.71	2.85	$(1.57 \pm 0.04) \times 10^{-17}$	1.042
11.51	2000	3.40	2665	5.32	2.66	$(3.40 \pm 0.06) \times 10^{-17}$	1.039
10.51	2000	3.39	2709	4.89	2.44	$(3.50 \pm 0.09) \times 10^{-17}$	1.027
9.54	2000	3.46	2831	4.49	2.13	$(1.71 \pm 0.05) \times 10^{-16}$	1.018
9.19	2000	3.53	2924	4.37	2.19	$(2.28 \pm 0.13) \times 10^{-16}$	1.022
7.80	2000	3.61	3061	3.76	1.88	$(4.12 \pm 0.11) \times 10^{-16}$	1.016
7.54	2000	3.64	3103	3.65	1.82	$(3.49 \pm 0.08) \times 10^{-16}$	1.015
6.04	2000	3.74	3269	2.97	1.48	$(9.27 \pm 0.27) \times 10^{-16}$	1.005
5.51	2000	3.76	3307	2.72	1.36	$(8.49 \pm 0.28) \times 10^{-16}$	1.005
5.10	2000	3.83	3425	2.54	1.27	$(1.37 \pm 0.08) \times 10^{-15}$	0.999
				SO_2 (499.8 ppm)			
15.03	2000	3.14	2340	16.6	3.32	$(2.65 \pm 0.08) \times 10^{-18}$	1.086
13.08	2000	3.22	2465	14.7	2.94	$(8.59 \pm 0.16) \times 10^{-18}$	1.079
12.53	2000	3.27	2539	14.2	2.85	$(1.37 \pm 0.03) \times 10^{-17}$	1.072
12.15	2000	3.33	2622	14.0	2.79	$(2.12 \pm 0.05) \times 10^{-17}$	1.081
10.82	2000	3.39	2709	12.6	2.51	$(3.03 \pm 0.06) \times 10^{-17}$	1.078
11.08	2125	3.44	2784	13.0	2.60	$(3.61 \pm 0.05) \times 10^{-17}$	1.107
9.06	2000	3.48	2856	10.7	2.14	$(1.18 \pm 0.04) \times 10^{-16}$	1.092
8.44	2000	3.54	2943	10.1	2.02	$(1.88 \pm 0.08) \times 10^{-16}$	1.086
7.53	2000	3.59	3028	9.05	1.81	$(2.99 \pm 0.07) \times 10^{-16}$	1.046
7.35	2000	3.68	3166	8.94	1.79	$(3.53 \pm 0.13) \times 10^{-16}$	1.024
5.92	2000	3.73	3254	7.26	1.45	$(5.86 \pm 0.50) \times 10^{-16}$	1.015
5.53	2000	3.77	3322	6.81	1.36	$(8.18 \pm 0.68) \times 10^{-16}$	1.011
				SO_2 (698.1 ppm)			
17.52	2000	3.07	2263	26.4	3.79	$(7.48 \pm 0.33) \times 10^{-19}$	1.148
15.12	2000	3.14	2358	23.3	3.33	$(2.65 \pm 0.11) \times 10^{-18}$	1.071
14.13	2000	3.20	2441	22.0	3.16	$(4.62 \pm 0.08) \times 10^{-18}$	1.136
16.58	2250	3.26	2519	26.0	3.74	$(7.50 \pm 0.16) \times 10^{-18}$	1.117
12.50	2000	3.33	2628	20.0	2.86	$(1.49 \pm 0.02) \times 10^{-17}$	1.088
				SO_2 (900.2 ppm)			
17.06	2000	3.03	2188	33.1	3.67	$(4.87 \pm 0.48) \times 10^{-19}$	1.170
16.53	2000	3.06	2237	32.3	3.59	$(8.95 \pm 0.48) \times 10^{-19}$	1.201
15.03	2000	3.13	2335	29.9	3.32	$(2.28 \pm 0.08) \times 10^{-18}$	1.184
13.52	2000	3.21	2441	27.3	3.03	$(6.16 \pm 0.18) \times 10^{-18}$	1.162
12.51	2000	3.26	2524	25.6	2.84	$(1.18 \pm 0.04) \times 10^{-17}$	1.168
12.11	2000	3.33	2617	24.9	2.78	$(1.79 \pm 0.03) \times 10^{-17}$	1.206
11.80	2000	3.39	2715	24.6	2.74	$(2.82 \pm 0.08) \times 10^{-17}$	1.103
9.05	2000	3.48	2856	19.1	2.14	$(7.96 \pm 0.37) \times 10^{-17}$	1.061

[a] P_1, pressure of reactant gas mixture; P_4, pressure of driver gas; M_s, Mach number; T_5, temperature of reaction. Concentrations are in molecule cm^{-3}; k_{1a} are fitted with kinetic modeling, and k'_{1a} are derived from pseudo-first-order kinetics.

Values of k_{1a} determined with various concentrations of SO_2 at various temperatures are plotted in Figure 3; comparison of results of previous reports is shown in Figure 4 with lines of various types drawn only for their respective investigated range of temperature. Our data support previous reports of greater rate coefficients; they agree well with those of Plach and Troe[6] (designated PT in Figures 3 and 4) in the overlapping range of temperature 3000−4249 K. Results of Kiefer[7] are also within

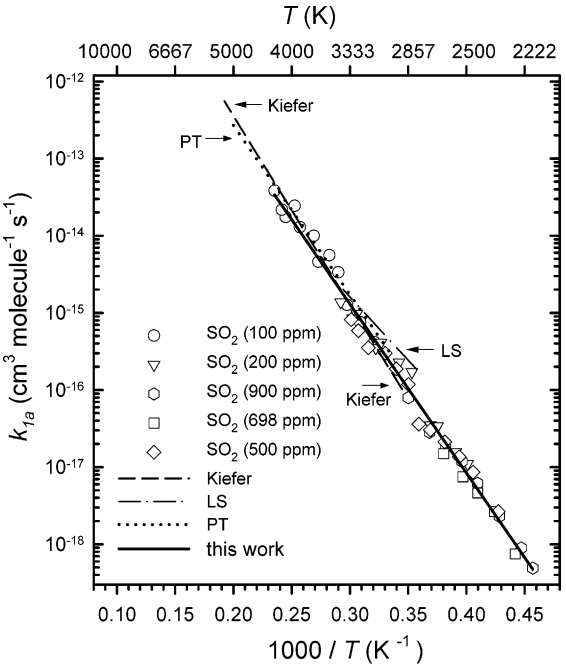

Figure 3. Arrhenius plots of k_{1a} for the reaction $SO_2 \rightarrow O + SO$. Our fitted equation is shown as a solid line, and previous results are shown as dotted (Plach and Troe),[6] dashed (Kiefer)[7] and dot−dashed (Levitt and Sheen)[2] lines.

experimental uncertainties of ours. At temperatures below 3000 K, rate coefficients reported by Levitt and Sheen[2] (designated LS) are slightly greater than ours. Results of Just and Rimpel (JR)[9] and Grillo et al. (GRS)[10] are smaller than our data by a factor of 1.3−4.2. We extended the temperature range of investigation down to 2188 K.

Fitting our results yields the expression

$$k_{1a}(T) = (4.86 \pm 1.31) \times 10^{-9} \exp[-(50450 \pm 730)/T]\ \mathrm{cm^3\ molecule^{-1}\ s^{-1}} \quad (23)$$

in which listed errors represent one standard deviation of the fit. Comparing with previous reports listed in Table 1, we found that both the preexponential factor A_0 and the activation energy E_a determined in our work agree with those reported by Plach and Troe,[6] who monitored UV absorption of SO_2 free from interference of SO. Rate coefficients reported by Kiefer[7] are also within experimental uncertainties of ours, but their E_a and A_0 values are greater than ours. The activation energy $E_a/R = 58600 \pm 2300$ K reported by Just and Rimple,[9] who employed a method similar to ours, is about 14% greater than ours; it is unclear why the errors are greater than expected experimental uncertainties. Previous reports of smaller rate coefficients,[3−5] although having a similar E_a, are clearly in error; the possibility that the absorption of SO interferes with that of SO_2 has been discussed previously.[6]

4.3. Formation of S Atoms and Kinetics of SO + O → S + O_2. Figure 5 shows a temporal profile of S atoms during pyrolysis of SO_2 at 3369 K; about 12% of S atoms are produced in ∼300 μs under such experimental conditions. The concentration of S atoms decreases as temperature decreases and becomes nearly undetectable ∼2258 K, as shown in trace B of Figure 6. Production of S atoms might result from pyrolysis of SO_2 through a direct channel

$$SO_2 \rightarrow S + O_2 \quad (1b)$$

or through further pyrolysis of the product SO

$$SO \xrightarrow{M} S + O \quad (13)$$

or through possible secondary reactions

$$O + SO \rightarrow S + O_2 \quad (10b)$$

$$SO + SO \rightarrow S + SO_2 \quad (12)$$

According to literature values of rate coefficients listed in the previous section, reactions 12 and 13 contribute little to the formation of S atoms. Some experiments were carried out with a mixture of N_2O, SO_2, and Ar, for which O atoms were also

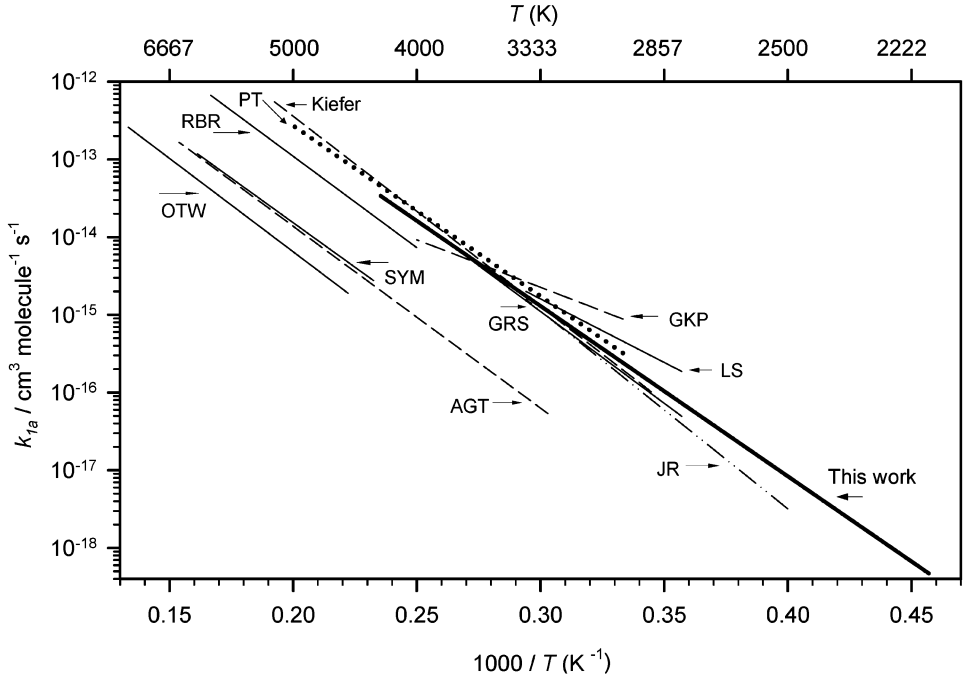

Figure 4. Comparison of reported values of k_{1a} for the reaction $SO_2 \rightarrow O + SO$. Each character represents the first letter of the author's last name; see Table 1 for references. Lines are drawn for the temperature range of study.

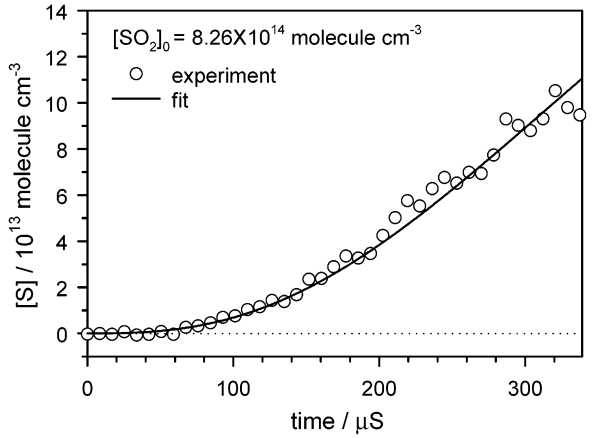

Figure 5. Representative temporal profile of [S] observed for pyrolysis of a sample containing SO_2 (350 ppm) and Ar. $T = 3369$ K and $P = 2.36 \times 10^{18}$ molecule cm^{-3}. The solid line represents fitted results using the model described in text.

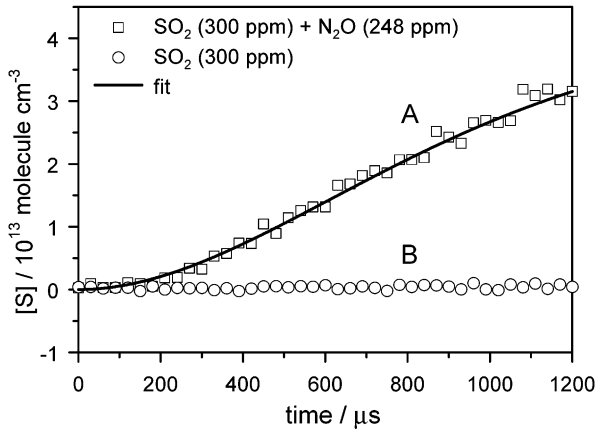

Figure 6. Temporal profiles of [S] observed for a sample, containing SO_2 (300 ppm) and Ar, heated by the shock wave to $T = 2258$ K and $P = 3.72 \times 10^{18}$ molecule cm^{-3}. (A) with N_2O (248 ppm); (B) without N_2O.

produced through thermal decomposition of N_2O. Under such conditions, [O] was much greater than when only SO_2 was present. Figure 6 compares temporal profiles of S atoms for a mixture containing SO_2 (300 ppm) with no N_2O and one containing SO_2 (300 ppm) and N_2O (248 ppm), both heated to ~2258 K. Without N_2O scarcely any S atom was detectable at this temperature, whereas with N_2O producing [O], production of S was enhanced, indicating the importance of reaction 10b.

We modeled observed temporal profiles of [S] with reactions 1a and 9−14 and reactions

$$S + O_2 \rightarrow SO + O \quad (24)$$

$$S + O \xrightarrow{M} SO \quad (25)$$

$$S + S \xrightarrow{M} S_2 \quad (26)$$

with literature values of rate coefficients

$$k_{24}(T) = 1.32 \times 10^{-10} \exp(-5075/T) \text{ cm}^3 \text{ molecule}^{-1} \text{ s}^{-1} \quad \text{(ref 36)} \quad (27)$$

$$k_{25}(T) = 3.55 \times 10^{-37} T^{0.7231} \exp(9658/T) \text{ cm}^6 \text{ molecule}^{-2} \text{ s}^{-1} \quad \text{(ref 6)} \quad (28)$$

TABLE 3: Experimental Conditions and Rate Coefficient k_{10b} for the Reaction O + SO → S + O_2[a]

P_1/ Torr	P_4/ Torr	M_s	T_5/ K	$[SO_2]$/ 10^{14}	[Ar]/ 10^{18}	$[N_2O]$/ 10^{14}	$k_{10b}/10^{-12}$ cm^3 molecule^{-1} s^{-1}
				SO_2 (350.0 ppm)			
10.01	2000	3.48	2843	8.26	2.36	0.00	2.47 ± 0.04
10.03	2250	3.57	2988	8.40	2.40	0.00	2.58 ± 0.05
10.01	2350	3.64	3109	8.40	2.42	0.00	3.03 ± 0.06
10.10	2550	3.77	3314	8.71	2.49	0.00	4.04 ± 0.06
9.53	2500	3.80	3369	8.26	2.36	0.00	3.73 ± 0.07
9.52	2500	3.81	3385	8.26	2.36	0.00	3.44 ± 0.06
				SO_2 (499.3 ppm)			
10.05	2250	3.54	2943	12.0	2.40	0.00	3.21 ± 0.04
10.04	2250	3.55	2962	11.9	2.39	0.00	2.71 ± 0.06
10.10	2500	3.69	3195	12.3	2.46	0.00	3.23 ± 0.06
9.51	2500	3.39	3314	11.7	2.34	0.00	3.75 ± 0.06
9.54	2500	3.46	3330	11.8	2.35	0.00	3.82 ± 0.06
				SO_2 (100.2 ppm) and N_2O (247.7 ppm)			
17.03	2000	3.04	2212	3.69	3.68	9.12	1.23 ± 0.02
17.00	2000	3.05	2224	3.69	3.68	9.13	1.25 ± 0.02
17.04	2000	3.10	2296	3.75	3.74	9.26	1.67 ± 0.02
16.52	2250	3.17	2394	3.69	3.68	9.11	1.95 ± 0.04
16.53	2250	3.21	2441	3.71	3.71	9.18	1.75 ± 0.02
16.51	2250	3.23	2470	3.73	3.72	9.21	1.90 ± 0.04
16.04	2250	3.28	2544	3.66	3.65	9.06	2.04 ± 0.03
16.02	2250	3.29	2564	3.66	3.65	9.05	2.19 ± 0.04
15.56	2250	3.32	2601	3.57	3.57	8.84	1.90 ± 0.03
15.53	2500	3.39	2709	3.62	3.61	8.94	2.19 ± 0.03
10.09	2250	3.58	3008	2.43	2.42	5.99	3.05 ± 0.04
10.02	2500	3.66	3138	2.44	2.43	6.03	3.53 ± 0.04
9.60	2500	3.69	3180	3.34	2.34	5.79	4.39 ± 0.05
10.03	2500	3.70	3202	2.45	2.45	6.07	3.01 ± 0.04
9.52	2500	3.77	3322	2.35	2.35	5.81	3.78 ± 0.06

[a] P_1, pressure of reactant gas mixture; P_4, pressure of driver gas; M_s, Mach number; T_5, temperature of reaction. Concentrations are in molecule cm^{-3}; k_{10b} are fitted with kinetic modeling.

$$k_{26}(T) = 2.83 \times 10^{-35} \exp(11300/T) \text{ cm}^6 \text{ molecule}^{-2} \text{ s}^{-1} \quad \text{(refs 32 and 39)} \quad (29)$$

and found satisfactory agreement between the observed ones with the predicted profiles. Rate coefficients k_{25} and k_{26} were derived by reported rate coefficients of their reverse reactions and equilibrium constants. The temporal profile of S atoms fit poorly with a model in which reaction 1b replaces reaction 10b. S atoms produced during pyrolysis of SO_2 clearly arise mainly from reaction 10b; the contribution of direct pyrolysis (reaction 1b) is likely much smaller than reaction 10b. With modeling, we estimated that $k_{1a}/k_{1b} > 100$ for $T > 3300$ K.

We modeled observed temporal profiles of [S] with reactions 1a, 9−14, and 24−26 with FACSIMILE;[38] rate coefficients except for reaction 10b were held constant, and the second-order rate coefficient of the title reaction, k_{10b}, was varied to yield the best fit. Experimental conditions and values of k_{10b} for 26 measurements at various initial concentrations ($[SO_2]$ = 100−499 ppm and $[N_2O]$ = 0 or 248 ppm in Ar) in the temperature range 2212−3385 K are summarized in Table 3. Values of k_{10b} at various temperatures are plotted in Figure 7. To our knowledge, there is no previous report on the rate coefficient of this reaction. Values of k_{10b} were also estimated from rate coefficients of the reverse reaction, reaction 24, reported by Woiki and Roth,[36] and the equilibrium constant derived from literature values of $\Delta G(T)$ for corresponding species.[37] Derived rate coefficient

$$k_{10b}(T) = 3.63 \times 10^{-11} \exp[-(7700/T)] \text{ cm}^3 \text{ molecule}^{-1} \text{ s}^{-1} \quad (18)$$

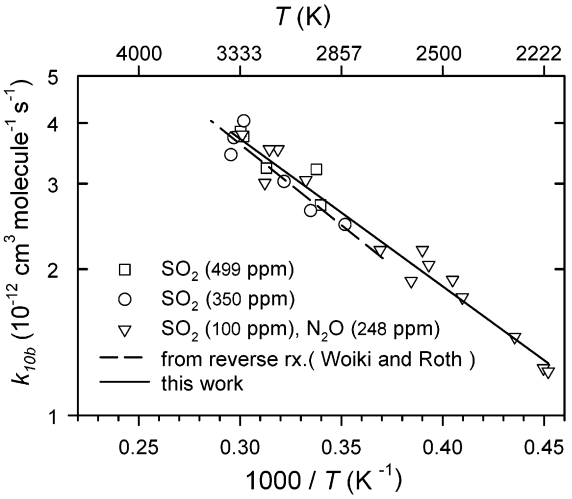

Figure 7. Arrhenius plots of k_{10b} for the reaction O + SO → S + O_2. Our fitted equation is shown as a solid line, and the dashed line represents values derived from experimental rates of the reverse reaction S + O_2 → SO + O and equilibrium constant; see text. Lines are drawn for the temperature range of study.

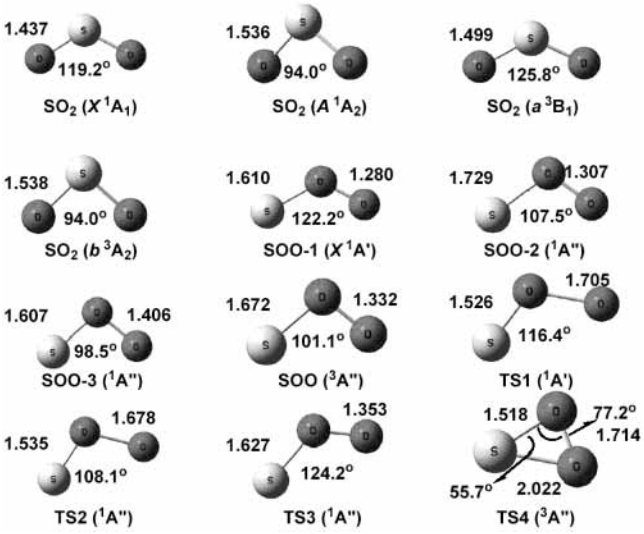

Figure 8. Optimized geometries of four transition states and reactants and products of the SO_2 system, with bond lengths in Å and bond angles in degree.

is shown in Figure 7 as a dashed line drawn only for their temperature range of investigation, 2732−3463 K, for comparison. Fitting our results to an Arrhenius equation yields

$$k_{10b}(T) = (3.0 \pm 0.3) \times 10^{-11} \exp[-(6980 \pm 280)/T] \text{ cm}^3 \text{ molecule}^{-1} \text{ s}^{-1} \quad (30)$$

in which listed errors represent one standard deviation of the fit. Estimated errors for k_{10b} are ±25% because rate coefficients were derived from secondary reactions. When our experimental results are compared with eq 18, the agreement is satisfactory.

4.4. Potential-Energy Surfaces and Reaction Mechanism. Our preliminary calculations[40] show that there are many triplet and singlet intermediates and transition states involved in the reaction of SO(X $^3\Sigma^-$) + O(^{3}P) to produce S(^{3}P) + O_2(X $^3\Sigma_g^-$). In this paper, only relevant low-lying energy channels are presented and discussed. The optimized geometries of the reactants, intermediates, transition states, and products are shown in Figure 8. The energy diagram calculated with the G2M(RCC2)//B3LYP/6-311+G(3df) method is presented in Figure 9. Reaction paths involving transition states with energies greater than 15 kcal mol^{-1} relative to O + SO are not shown; a complete description of the theoretical study on the SOO system will be published separately.[40] Predicted vibrational wavenumbers and rotational constants as well as available experimental data[41−45] for the species involved are summarized in Table 4. The results indicate that the predicted vibrational wavenumbers are underestimated by 0.2−2.3% from experimental values.

TABLE 4: Vibrational Wave Numbers and Rotational Parameters Calculated at the B3LYP/6-311+G(3df) Level

species	B/GHz	vibrational wavenumbers/cm^{-1}
SO ($^3\Sigma^-$)	21.4	1156.7 (1136.7)[a]
SO_2 (X $^1A_1$)	59.8, 10.3, 8.8	519.1 (517.7), 1178.1 (1151.4), 1376.9 (1361.8)[b]
SO_2 (A $^1A_2$)	28.8, 12.5, 8.7	414.7, 453.8, 1031.5
SO_2 (a $^3B_1$)	67.8, 8.9, 7.8	373.9 (362), 946.3 (904), 955.3 (967)[c]
SO_2 (b $^3A_2$)	28.7, 12.5, 8.7	414.9, 586.7, 1027.8
SOO-1 ($^1A'$)	95.3, 6.9, 6.4	492.9, 800.9 (739.9), 1142.1 (1006.1)[d]
SOO-2 ($^1A''$)	60.2, 7.1, 6.4	209.2, 551.7, 1130.6
SOO-3 ($^1A''$)	47.3, 8.5, 7.2	353.7, 650.8, 921.8
SOO ($^3A''$)	52.2, 8.0, 6.9	280.6, 590.4, 1050.2
TS1	59.7, 6.2, 5.6	685.4i, 322.2, 972.5
TS2	48.6, 6.8, 6.0	687.1i, 218.4, 970.4
TS3	93.9, 6.4, 6.0	328.8i, 678.5, 801.9
TS4	27.2, 11.4, 8.0	845.7i, 320.9, 1065.2
O_2 ($^3\Sigma_g^-$)	43.6	1645.3
SO_2 (b $^3A_2$)	43.0, 10.8, 8.1[e]	(780, 700, 300)[c]

[a] Values in parentheses are experimental values from ref 42. [b] Values in parentheses are experimental values from ref 41. [c] Values in parentheses are experimental values from ref 43. [d] Values in parentheses are experimental values from ref 45. [e] Rotational parameters are experimental values from ref 44.

A. Ground-State SO_2 (X $^1A_1$). The most stable conformation of SO_2 has C_{2v} symmetry; its ground electronic state ($^1A_1$) has been extensively investigated experimentally[41,46] and theoretically[45,47] with various methods. At the B3LYP/6-311+G(3df) level, the optimized S−O bond length is 1.437 Å, which can be compared with 1.448, 1.462, 1.471, and 1.450 Å, obtained from calculations at the CCSD(T)/TZ2P(f,d),[47] CCSD(T)/DZP,[47] BP86/cc-pVTZ,[45] and B3LYP/cc-pVTZ levels,[45] respectively, and the experimental value of 1.431 Å.[46] A calculated OSO bond angle of 119.2° agrees well with the experimental value of 119.3°. The enthalpy of formation for SO_2 is predicted to be −69.2 kcal mol^{-1} at the G2M(RCC2) level at 0 K, which is in good agreement with the experimental value, −70.3 ± 0.3 kcal mol^{-1}.[37] The calculated dissociation energy D_0(O−SO), 129.4 kcal mol^{-1}, for the ground-state SO_2 agrees with the experimental value of 130.5 ± 0.4[37] and 130.7 kcal mol^{-1}.[48]

B. Low-Lying States A $^1A_2$, a $^3B_1$, and b $^3A_2$ of SO_2. Figures 8 and 9 also present the structures and energies of three low-lying states, A $^1A_2$, a $^3B_1$, and b $^3A_2$, of SO_2 which are bound states with no barriers for their dissociation to the lowest asymptotes of SO($^3\Sigma^-$) + O(^{3}P). The A $^1A_2$ state is predicted to lie 73.4 kcal mol^{-1} above the ground X $^1A_1$ state, which is smaller than the experimental value, 79.8 kcal mol^{-1}.[49] The a $^3B_1$ state is predicted to lie 75.5 kcal mol^{-1} above the ground X $^1A_1$ state, which agrees with the value 75.2 kcal mol^{-1} obtained by Katagiri et al.[25] at the MRCI/cc-pVDZ level; they are slightly greater than the experimental data, 73.6 kcal mol^{-1}.[43,50] For the b $^3A_2$ state, the calculated result lies above the X $^1A_1$ state by 76.8 kcal mol^{-1}, which is close to the experimental value, 77.3 kcal mol^{-1}.[43,44]

C. ^3S + $^3O_2$ Formation. Figure 9 shows that S(^{3}P) + O_2(X $^3\Sigma_g^-$) can be formed via singlet and triplet SOO intermediates.

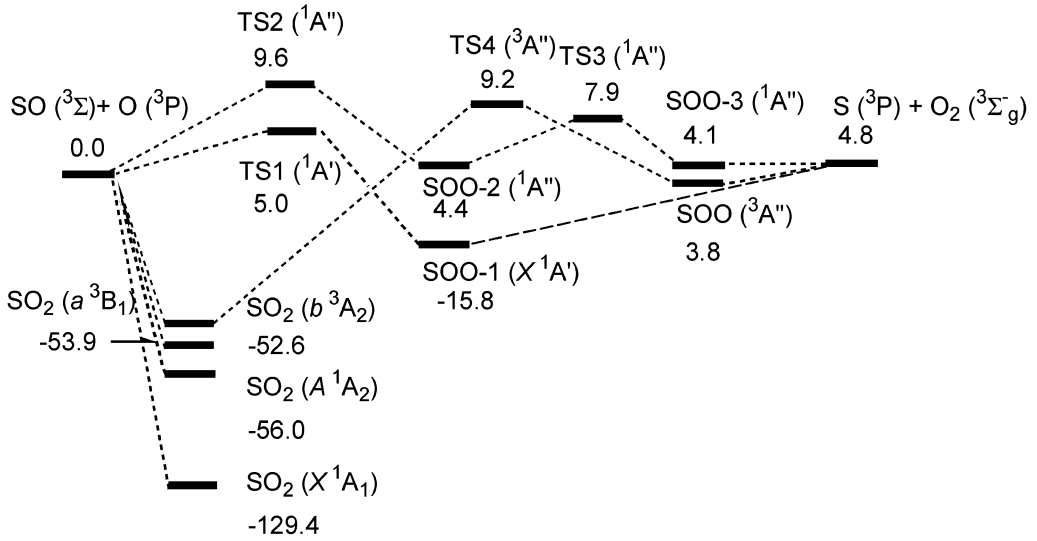

Figure 9. Potential-energy diagram for reactions 1a and 1b based on energies calculated with G2M(RCC2)//B3LYP/6-311+G(3df). Energies are listed in kcal mol^{-1}. Reaction paths with transition state energies greater than 15 kcal mol^{-1} above O + SO are not shown; a complete diagram is shown in ref 40.

The singlet channels proceed via two surfaces, ^{1}A′ and ^{1}A″. The entrance barriers for ^{1}A′ and ^{1}A″ from SO + O are 5.0 (TS1) and 9.6 kcal mol^{-1} (TS2), respectively; the ^{1}A′ intermediate (SOO-1) is more stable than those of ^{1}A″ (SOO-2 and SOO-3). The predicted energy of SOO-1, 113.6 kcal mol^{-1} above SO_2 (X ^{1}A$_1$), is similar to a value of 117 kcal mol^{-1} predicted by Kellogg and Schaefer[47] but greater than a value of 105 kcal mol^{-1} predicted by Dunning and Raffenetti,[51] who employed a two-reference CI method with generalized valence-bond (GVB) natural orbitals. The triplet channel proceeds through the SO_2 (b ^{3}A$_2$) intermediate followed by dissociation via TS4 to produce S + O_2. The predicted heat of reaction, 4.8 kcal mol^{-1}, for reaction 10b is close to the value obtained from JANAF, 5.5 kcal mol^{-1}.[37]

4.5 Calculations of Rate Coefficients. Calculations based on variational transition-state and RRKM theories were carried out with the Variflex code[26] for the following reactions:

$$SO_2 \rightarrow O(^3P) + SO(^3\Sigma^-) \qquad (1a)$$

$$O(^3P) + SO(^3\Sigma^-) \xrightarrow{M} SO_2 \qquad (10a)$$

$$O(^3P) + SO(^3\Sigma^-) \rightarrow S(^3P) + O_2(^3\Sigma_g^-) \qquad (10b)$$

The energies used in the calculation are shown in Figure 9; vibrational wavenumbers and rotational parameters are listed in Table 4.

A. $SO_2 \rightarrow SO + O$. The decomposition of SO_2 to form O(^{3}P) and SO($^3\Sigma^-$) proceeds without a well-defined transition state due to the absence of an intrinsic reaction barrier. To predict the dissociation rate reliably, we implemented a flexible variational transition-state approach, originally developed by Marcus and co-workers,[52,53] into the Variflex code.[26] The dissociation energy for reaction 1a was calculated by increasing the S−O bond distance from its equilibrium value, 1.437 Å, to 4.0 Å at intervals 0.1 Å. Energies of A ^{1}A$_2$, a ^{3}B$_1$, and b ^{3}A$_2$ states were calculated similarly. Calculated energies were fitted to a Morse equation (eq 3) scaled to match the dissociation energy predicted at the G2M(RCC2) level of theory.[18] Values of β in the Morse potential were determined to be 2.779, 1.891, and 1.634 Å^{-1} for the X ^{1}A$_1$, A ^{1}A$_2$, and a ^{3}B$_1$ states, respectively; the value of 1.634 Å^{-1} predicted for the a ^{3}B$_1$ state was also used for the b ^{3}A$_2$ state in the calculation. States A ^{1}A$_2$, a ^{3}B$_1$, and b ^{3}A$_2$ lie below the dissociation limit of SO_2 by more than 52 kcal mol^{-1}; contributions of these states to the total rate coefficient for dissociation are calculated by multiplying rate coefficients of decomposition by relative populations of each state assuming that these electronic states are strongly mixed.

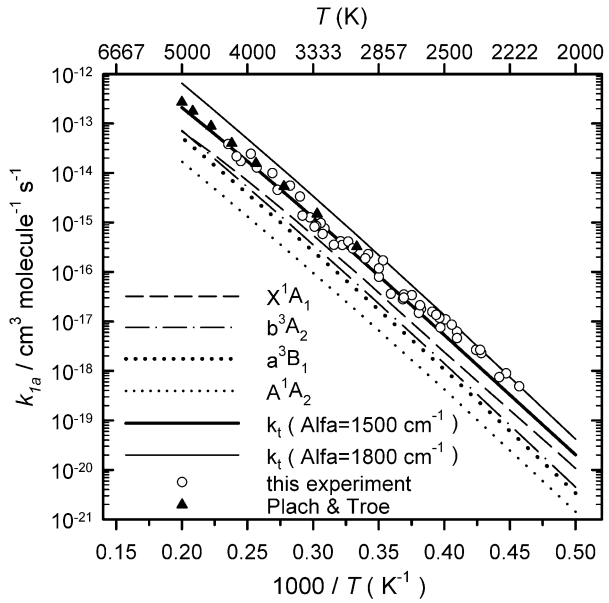

Figure 10. Comparison of predicted rate coefficient k_{1a} (solid line) for $SO_2 \rightarrow O + SO$ with experimental data (○, this work; ▲, Plach and Troe[6]). Contributions from decomposition via various electronic states of SO_2 are shown with broken lines as indicated in the legend.

The Lennard-Jones (LJ) parameters required for the RRKM calculations, $\epsilon/k = 328.5$ and 113.5 K, and $\sigma = 4.102$ and 3.465 Å, for SO_2 X ^{1}A$_1$ and Ar, respectively, are taken from ref 54. The LJ parameters for other states of SO_2 were assumed to be the same as those of the X ^{1}A$_1$ state.

Predicted rate coefficients of decomposition of SO_2 and partial contributions from the four electronic states of SO_2 are compared with experimental results in Figure 10. To reproduce experimental data satisfactorily, a larger $\langle \Delta E_{down} \rangle$ has to be used for

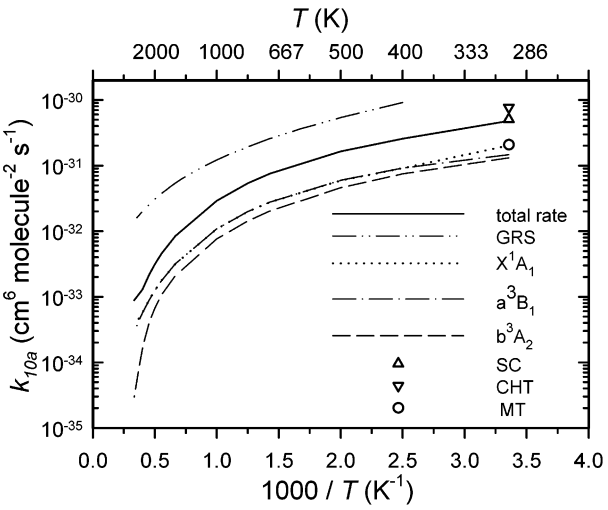

Figure 11. Comparison of predicted rate coefficient k_{10a} (solid line) for O + SO → SO_2 with experimental data (○, Miyazaki and Takahashi;[55] ▽, Cobos et al.;[56] △, Singleton and Cvetanovic[33]). An estimate of temperature dependence of k_{10b} by Grillo et al.[10] is shown with broken lines.

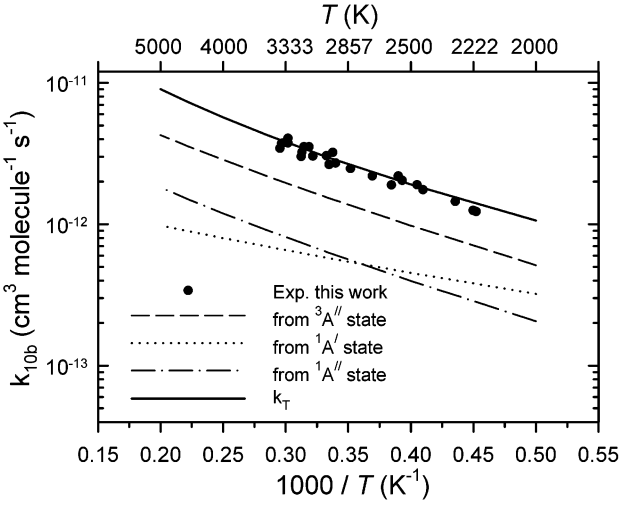

Figure 12. Comparison of the predicted rate coefficient k_{10b} for the reaction SO + O → S + O_2. Contributions from different channels are shown as broken lines, as indicated in the legend.

this system; the values are temperature dependent and can be approximated by

$$\langle \Delta E_{down} \rangle = 560\ (T/298)^{0.43}\ \text{cm}^{-1} \tag{31}$$

The best predicted total rate coefficients (thick line in Figure 10) can be expressed in an Arrhenius form

$$k_{1a}(T) = 4.71 \times 10^{-8} \exp\,[-(55190/T)]\ \text{cm}^3\ \text{molecule}^{-1}\ \text{s}^{-1} \tag{32}$$

Predicted activation energy of $E_a/R = 55190$ K is ∼9% greater than our experimental value, but within experimental uncertainties.

It should be pointed out that SO_2 cannot effectively dissociate to give S + O_2; this product channel proceeds via tight 3-centered TSs producing SOO intermediates with relatively high barriers. The lowest isomerization barrier, $^3SO_2$ ($^3A_2$) → ^{3}SOO ($^3A''$) is 9.2 kcal mol^{-1} above O + SO (Figure 9). For other possible isomerization processes, the barriers are even higher; for example, the barriers for SO_2 ($^1A_2$) → ^{1}SOO ($^1A''$) and SO_2 ($^1A_1$) → ^{1}SOO ($^1A'$) are 15.2 and 19.5 kcal mol^{-1} above O + SO, respectively (not shown in Figure 9). Therefore, the reaction channel (1b) for pyrolysis of SO_2 to form S and O_2 is negligible. Our experimental observation of temporal profiles for production of S atoms is consistent with the dominant secondary reaction

$$\text{O} + \text{SO} \rightarrow \text{S} + \text{O}_2 \tag{10b}$$

rather than with direct formation via reaction 1b, agreeing with theoretical prediction.

B. O + SO → SO_2. Figure 11 compares predicted and experimental rate coefficients for the association reaction 10a; $\langle \Delta E_{down} \rangle = 400$ cm^{-1} was employed for collisional stabilization. Formation of SO_2 in its X $^1A_1$, a $^3B_1$, and b $^3A_2$ states contributes ∼42, 31, and 27% to the total rate coefficients at 298 K and changes to ∼37, 37, and 26%, respectively, at 1000 K. The results show that the total rate coefficient decreases with increasing temperature, as expected for an association reaction. The predicted rate coefficient at 298 K, 4.8 × 10^{-31} cm^6 molecule^{-2} s^{-1}, agrees satisfactory with a recommended value for M = Ar by Singleton and Cvetanovic,[33] 5.1 × 10^{-31} cm^6 molecule^{-2} s^{-1}, but deviates from values of (2.07 ± 0.23) × 10^{-31} cm^6 molecule^{-2} s^{-1} by Miyazaki and Takahashi[55] and 7.69 × 10^{-31} cm^6 molecule^{-2} s^{-1} (M = N_2) by Cobos et al.[56] The temperature dependence of the rate coefficient may be expressed as

$$k_{10a}(T) = (4.82 \pm 0.05) \times 10^{-31}(T/298)^{-2.17\pm0.03}\ \text{cm}^6\ \text{molecule}^{-2}\ \text{s}^{-1} \tag{33}$$

for the temperature range 298−3000 K, in satisfactory agreement with the expression 9.3 × 10^{-31}(T/298)$^{-1.84}$ cm^6 molecule^{-2} s^{-1} reported by Grillo et al.[10] based on an equilibrium constant derived from Gibb's free energies, the previously reported values of k_{1a}[9,10] and an erroneous value of k_{10a} at 298 K.

C. O + SO → S + O_2. As described in the previous section, S(^{3}P) + O_2(X $^3\Sigma_g^-$) can be formed via $^1A'$, $^1A''$, and $^3A''$ PES (see Figure 9). The predicted individual and total rate constants are presented in Figure 12 for comparison with experimental values determined in this work. It is readily seen that combination of three reaction channels can well reproduce experimental data. The predicted total rate constant in the temperature range of 2000−5000 K can be expressed as

$$k_{10b}(T) = 3.92 \times 10^{-17}\ T^{1.51} \exp\,[-(2537/T)]\ \text{cm}^3\ \text{molecule}^{-1}\text{s}^{-1} \tag{34}$$

or

$$k_{10b}(T) = 3.4 \times 10^{-11} \exp\,[-(7122/T)]\ \text{cm}^3\ \text{molecule}^{-1}\text{s}^{-1} \tag{35}$$

in close agreement with the experimental value

$$k_{10b}(T) = (3.0 \pm 0.3) \times 10^{-11} \exp\,[-(6980 \pm 280)/T]\ \text{cm}^3\ \text{molecule}^{-1}\ \text{s}^{-1} \tag{30}$$

5. Conclusion

Rate coefficients for pyrolysis of SO_2 to form O and SO in the temperature range 2188−4249 K were determined using a diaphragmless shock tube with atomic resonance absorption detection of O and S atoms. Our results are consistent with measurements by Plach and Troe but show a slightly smaller

preexponential factor. Rate coefficients may be expressed with the equation $k_{1a}(T) = (4.86 \pm 1.31) \times 10^{-9}$ exp $[-(50450 \pm 730)/T]$ cm^3 molecule^{-1} s^{-1}, in which listed errors represent one standard deviation in fitting. Theoretical calculations indicate that the reaction path leading to the formation of S + O_2 is unimportant, but decomposition via electronically excited states a $^3B_1$ and b $^3A_2$ contributes significantly; the total rate coefficients agree with experiments throughout the temperature range of investigation. The rate coefficient of the reverse reaction SO + O → SO_2 is predicted to be $k_{10a}(T) = (4.82 \pm 0.05) \times 10^{-31}(T/298)^{-2.17\pm0.03}$ cm^6 molecule^{-2} s^{-1} for the temperature range 298−3000 K. Experimental observation of S atoms fits satisfactorily with a model involving a secondary reaction O + SO → S + O_2; the rate coefficient $k_{10b}(T) = (3.0 \pm 0.3) \times 10^{-11}$ exp$[-(6980 \pm 280)/T]$ cm^3 molecule^{-1} s^{-1} was determined for the first time. The result can be quantitatively accounted for theoretically based on the PES computed at the G2M(RCC2)//B3LYP/6-311+(3df) level of theory.

Acknowledgment. Y.P.L. thanks the National Science Council of Taiwan (Grant No. NSC 91-2119-M-007-003) and the MOE Program for Promoting Academic Excellence of Universities (Grant No. 89-FA04-AA) for support. R.S.Z. and M.C.L. thank the Office of Naval Research, U.S. Navy (Contract No. N00014-89-J1949) for support. M.C.L. also acknowledges the support from the National Science Council of Taiwan for a distinguished visiting professorship at the Center for Interdisciplinary Molecular Sciences, National Chiao Tung University, Hsinchu, Taiwan.

References and Notes

(1) Gaydon, A. G.; Kimbell, G. H.; Palmer, H. B. *Proc. R. Soc. A* **1963**, *276*, 461.
(2) Levitt, B. P.; Sheen, D. B. *Trans. Faraday Soc.* **1967**, *63*, 2955.
(3) Olschewski, H. A.; Troe, J.; Wagner, H. Gg. *Z. Phys. Chem. Neue Folge* **1965**, *44*, 173.
(4) Astholz, D. C.; Glänzer, K.; Troe, J. *Proc. 11th International Symposium on Shock Tubes and Shock Waves*; University of Washington Press: Seattle, WA, 1978; p 232.
(5) (a) Saito, K.; Yokubo, T.; Murakami, I. *J. Chem. Phys.* **1980**, *73*, 3017. (b) Saito, K.; Yokubo, T.; Higashihara, T.; Murakami, I. *Bull. Chem. Soc. Jpn.* **1980**, *53*, 1439.
(6) Plach, H. J.; Troe, J. *Int. J. Chem. Kinet.* **1984**, *16*, 1531.
(7) Kiefer, J. H. *J. Chem. Phys.* **1975**, *62*, 1354.
(8) (a) Raju, M. T.; Babu, S. V.; Rao, Y. V. C.; Rao V. S. *Proc. 13th International Symposium on Shock Tubes and Shock Waves*; Magnes Press: Jerusalem, 1982; p 570. (b) Raju, M. T.; Babu, S. V.; Rao V. S. *Chem. Phys.* **1980**, *48*, 411.
(9) Just, Th.; Rimpel, G. *Proc. 11th International Symposium on Shock Tubes and Shock Waves*; University of Washington Press: Seattle, WA, 1978; p 226.
(10) Grillo, A.; Reed, R.; Slack, M. W. *Proc. 12th International Symposium on Shock Tubes and Shock Waves*; Magnes Press: Jerusalem, 1980; p 486. (b) Grillo, A.; Reed, R.; Slack, M. W. *J. Chem. Phys.* **1979**, *70*, 1634.
(11) Koshi, M.; Yoshimura, M.; Fukuda, K.; Matsui, H.; Saito, K.; Watanabe, M.; Imamura, A.; Chen, C. *J. Chem. Phys.* **1990**, *93*, 8703.
(12) Hsiao, C.-C.; Lee, Y.-P.; Wang, N. S.; Wang, J. H.; Lin, M. C. *J. Phys. Chem. A* **2002**, *106*, 10231.
(13) Greene, E. F.; Toennies, J. P. *Chemical Reactions in Shock Waves*; Academic Press: New York, 1964.
(14) Michael, J. V. *J. Chem. Phys.* **1989**, *90*, 189.
(15) Michael, J. V.; Sutherland, J. W. *Int. J. Chem. Kinet.* **1986**, *18*, 409.
(16) Becke, A. D. *J. Chem. Phys.* **1993**, *98*, 5648; **1992**, *96*, 2155; **1992**, *97*, 9173.
(17) Lee, C.; Yang, W.; Parr, R. G. *Phys. Rev. B* **1988**, *37*, 785.
(18) Mebel, A. M.; Morokuma, K.; Lin, M. C. *J. Chem. Phys.* **1995**, *103*, 7414.
(19) Gonzalez, C.; Schlegel, H. B. *J. Phys. Chem.* **1989**, *90*, 2154.
(20) Frisch, M. J.; Trucks, G. W.; Schlegel, H. B.; Scuseria, G. E.; Robb, M. A.; Cheeseman, J. R.; Zakrzewski, V. G.; Montgomery, J. A., Jr.; Stratmann, R. E.; Burant, J. C.; Dapprich, S.; Millam, J. M.; Daniels, A. D.; Kudin, K. N.; Strain, M. C.; Farkas, O.; Tomasi, J.; Barone, V.; Cossi, M.; Cammi, R.; Mennucci, B.; Pomelli, C.; Adamo, C.; Clifford, S.; Ochterski, J.; Petersson, G. A.; Ayala, P. Y.; Cui, Q.; Morokuma, K.; Malick, D. K.; Rabuck, A. D.; Raghavachari, K.; Foresman, J. B.; Cioslowski, J.; Ortiz, J. V.; Stefanov, B. B.; Liu, G.; Liashenko, A.; Piskorz, P.; Komaromi, I.; Gomperts, R.; Martin, R. L.; Fox, D. J.; Keith, T.; Al-Laham, M. A.; Peng, C. Y.; Nanayakkara, A.; Gonzalez, C.; Challacombe, M.; Gill, P. M. W.; Johnson, B. G.; Chen, W.; Wong, M. W.; Andres, J. L.; Head-Gordon, M.; Replogle, E. S.; Pople, J. A. *Gaussian 98*, revision A.6; Gaussian, Inc.: Pittsburgh, PA, 1998.
(21) MOLPRO is a package of ab initio programs written by Werner, H.-J.; Knowles, P. J. with contributions from Almlöf, J.; Amos, R. D.; Berning, A.; Cooper, D. L.; Deegan, M. J. O.; Dobbyn, A. J.; Eckert, F.; Elbert, S. T.; Hampel, C.; Lindh, R.; Lloyd, A. W.; Meyer, W.; Nicklass, A.; Peterson, K.; Pitzer, R.; Stone, A. J.; Taylor, P. R.; Mura, M. E.; Pulay, P.; Schütz, M.; Stoll, H.; Thorsteinsson, T.
(22) Tyrrell, J.; Kar, T.; Bartolotti, L. J. *J. Phys. Chem. A* **2001**, *105*, 4065.
(23) Murray, C. W.; Handy, N. C.; Amos, R. D. *J. Chem. Phys.* **1993**, *98*, 7145.
(24) Zhu, R. S.; Lin, M. C. *Chem. Phys. Lett.* **2002**, *354*, 217.
(25) Katagiri, H.; Sako, T.; Hishikawa, A.; Yazaki, T.; Onda, K.; Yamanouchi, K.; Yoshino, K. *J. Mol. Struct.* **1997**, *413*−*414*, 589.
(26) Klippenstein, S. J.; Wagner, A. F.; Dunbar, R. C.; Wardlaw, D. M.; Robertson, S. H. *VARIFLEX*, version 1.00; 1999.
(27) Gilbert, R. G.; Smith, S. C. *Theory of Unimolecular and Recombination Reaction*; Blackwell Scientific: Carlton, Australia, 1990.
(28) Holbrook, K. A.; Pilling, K. J.; Robertson, S. H. *Unimolecular Reactions*; Wiley: Chichester, U.K., 1996.
(29) Ross, S. K.; Sutherland, J. W.; Kuo, S.-C.; Klemm, R. B. *J. Phys. Chem. A* **1997**, *101*, 1104.
(30) Oya, M.; Shiina, H.; Tsuchiya, K.; Matsui, H. *Bull. Chem. Soc. Jpn.* **1994**, *67*, 2311.
(31) Shiina, H.; Miyoshi, A.; Matsui, H. *J. Phys. Chem. A* **1998**, *102*, 3556.
(32) Smith, O. I.; Tseregounis, S.; Wang, S.-N. *Int. J. Chem. Kinet.* **1982**, *14*, 679.
(33) Singleton, D. L.; Cvetanovic, R. J. *J. Phys. Chem. Ref. Data* **1988**, *17*, 1377.
(34) Tsang, W.; Hampson, R. F. *J. Phys. Chem. Ref. Data* **1986**, *15*, 1087.
(35) Schofield, K. *J. Phys. Chem. Ref. Data* **1973**, *2*, 25.
(36) Woiki, D.; Roth, P. *Int. J. Chem. Kinet.* **1995**, *27*, 59.
(37) Chase, M. W., Jr. NIST-JANAF Themochemical Tables, 4th ed. *J. Phys. Chem. Ref. Data* **1998**, *Monograph 9*, 1−1951.
(38) FACSIMILE is a computer software for modeling process and chemical reaction kinetics; AEA Technology: Oxfordshire, U.K.
(39) Higashihara, T.; Saito, K.; Murakami, I. *Bull. Chem. Soc. Jpn.* **1980**, *53*, 15.
(40) Zhu, R. S.; Lin, M. C.; Wu, Y.-J.; Lee, Y.-P. unpublished work.
(41) Shimanouchi, T., *Tables of Molecular Vibrational Frequencies Consolidated Volumed I*; National Bureau of Standards: Gaithersburg, MD, 1972; pp 1−160.
(42) Hopkins, A. G.; Brown, C. W. *J. Chem. Phys.* **1975**, *62*, 2511.
(43) Zen, C.-C.; Chen, I−C.; Lee, Y.-P. *J. Phys. Chem. A* **2000**, 104, 771.
(44) Huang, C. L.; Chen, I−C.; Merer, A. J.; Ni, C. K.; Kung, A. H. *J. Chem. Phys.* **2001**, *114*, 1187.
(45) Chen, L.-S.; Lee, C.-I; Lee, Y.-P. *J. Chem. Phys.* **1996**, *105*, 9454.
(46) Morino, Y.; Kikuchi, Y.; Saito, S.; Hirota, E. *J. Mol. Spectrosc.* **1964**, *13*, 95.
(47) Kellogg, C. B.; Schaefer, H. F., III. *J. Chem. Phys.* **1995**, *102*, 4177.
(48) Becker, S.; Braatz, C.; Lindner, J.; Tiemann, E. *Chem. Phys.* **1995**, *196*, 275.
(49) Hamada, Y.; Merer, A. J. *Can. J. Phys.* **1974**, *52*, 1443.
(50) Brand, J. C. D.; Jones, V. T.; di Lauro, C. *J. Mol. Spectrosc.* **1973**, *45*, 404.
(51) Dunning, T. H.; Raffenetti, R. C. *J. Am. Chem. Soc.* **1981**, *85*, 1350.
(52) Wardlaw, D. M.; Marcus, R. A. *Chem. Phys. Lett.* **1984**, *110*, 230; *J. Chem. Phys.* **1985**, *83*, 3462.
(53) Klippenstein, S. J.; Marcus, R. A. *J. Chem. Phys.* **1987**, *87*, 3410.
(54) Mourits, F. M.; Rummens, F. H. A. *Can. J. Chem.* **1977**, *55*, 3007.
(55) Miyazaki, S.; Takahashi, S. *Mem. Def. Acad. Math. Phys. Chem. Eng. (Yokosuka Jpn.)* **1971**, *11*, 307.
(56) Cobos, C. J.; Hippler, H.; Troe, J. *J. Phys. Chem.* **1985**, *89*, 1778.